

# Non-Linear Anisotropic Diffusion for Memory-Efficient Computed Tomography Super-Resolution Reconstruction (Supplemental Material)

Khaled Abujbara \* Ramzi Idoughi \* Wolfgang Heidrich

KAUST

Thuwal, Saudi Arabia

[first name].[family name]@kaust.edu.sa

## 1. Convergence Conditions

In the Regularization by Denoising (RED) framework, the denoiser engine ( $D(\cdot)$ ) should satisfy two conditions for guaranteed convergence [1]:

- Local homogeneity: we should verify that

$$\forall 0 \leq \epsilon \ll 1 : D((1 + \epsilon)\mathbf{x}) = (1 + \epsilon)D(\mathbf{x})$$

- Strong passivity: The Jacobian of the denoiser should satisfy

$$\eta(\nabla_{\mathbf{x}}D(\mathbf{x})) \leq 1,$$

where  $\eta(\cdot)$  is the spectral radius of a matrix.

In this section we will present numerical tests that we have performed in order to heuristically show that these two conditions are met by the Non-Linear Anisotropic Diffusion (NLAD) denoiser.

for our selected denoiser.

### 1.1. Local homogeneity

Following a similar approach to the original paper on RED approach [1], we provide an empirical evidence of the local homogeneity by plotting:  $D((1 + \epsilon)\mathbf{x})$  versus  $(1 + \epsilon)D(\mathbf{x})$ . We used a simulated Fresnel Zone Plate of size  $256 \times 256 \times 256$ , to which Gaussian noise is added ( $\sigma = 0.3$ ) (Figure 1). This resulting plot is shown in Figure 2, and demonstrates the required equality of the two terms.

### 1.2. Strong passivity

To show strong passivity, we computed the spectral radius of the Jacobian using the power iteration method. This is done following Algorithm 1.

---

\*Both authors contributed equally.

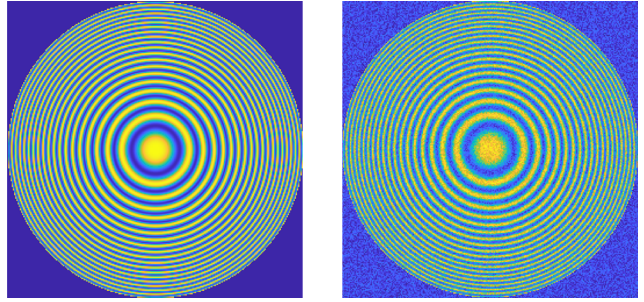


Figure 1: Fresnel Zone Plate data used for proving the local homogeneity and the strong passivity. Simulated FZP (left side) and The noisy FZP (right side).

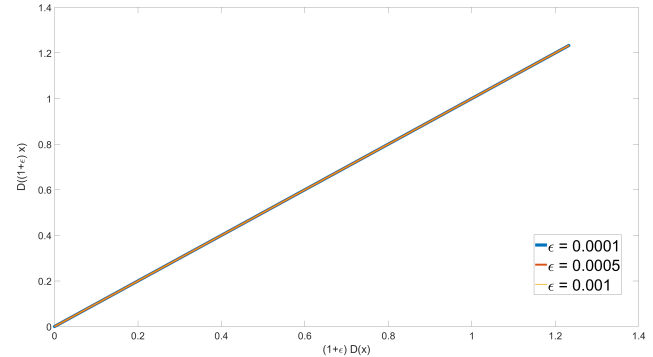


Figure 2: Plotting  $D((1 + \epsilon)\mathbf{x})$  versus  $(1 + \epsilon)D(\mathbf{x})$  shows clearly the local homogeneity for this data. Different values of  $\epsilon$  have been chosen.

For our experiment we choose the same input data (Noisy FZP) used for the local homogeneity experiment, with  $\epsilon = 0.001$ . Figure 3 shows the progression of this algorithm over multiple iterations. We notice that the spectral radius of the Jacobian of the denoiser converges to 1, which satisfies the strong passivity condition.

Table 1: Parameters used to run the baseline methods a for both synthetic and real datasets.

Method	Parameter	FZP2	FZP4	FZP8	Toothbrush	Ropeball	Fan
<b>SART</b>	Main loop iterations	15	15	20	13	5	12
	Momentum $\alpha$	0.3	0.3	0.3	0.1	0.1	0.009
<b>PSART-ATV</b>	Main loop iterations	15	15	15	8	6	7
	Nested prior iterations	1	1	1	1	1	1
	Nested SART iterations	3	3	3	2	2	3
	Prior parameter $\lambda$	0.003	0.003	0.003	0.1	0.08	0.08
<b>PSART-STP</b>	CP parameters $\mu, \tau$	0.15, 1.3e-4	0.15, 1.3e-4	0.15, 1.3e-4	0.1, 0.1	0.15, 0.13	0.15, 0.13
	Main loop iterations	25	25	14	12	5	7
	Nested prior iterations	1	1	1	1	1	1
	Nested SART iterations	3	3	3	2	2	3
	Prior parameter $\lambda$	0.3	0.03	0.03	0.5	0.3	1
	CP parameters $\mu, \tau$	0.3	0.3	0.3	0.3	0.1	0.13, 0.15

**Algorithm 1** Power iteration method applied on the Jacobian of the denoiser NLAD

---

**Require:**  $D(\cdot), \epsilon, \mathbf{x}, T$

- 1: Initialization:  $\mathbf{x}_0 \leftarrow \mathbf{x}$
- 2: **for all**  $t = 0 \dots T$  **do**
- 3:    $D_{\mathbf{x}_t} \leftarrow D(\mathbf{x}_t)$
- 4:    $D_{(1+\epsilon)\mathbf{x}_t} \leftarrow D((1 + \epsilon)\mathbf{x}_t)$
- 5:    $J_t \leftarrow \frac{D_{(1+\epsilon)\mathbf{x}_t} - D_{\mathbf{x}_t}}{\epsilon}$
- 6:    $\eta_t \leftarrow \frac{\|J_t \mathbf{x}_t\|}{\|\mathbf{x}_t\|}$
- 7:    $\mathbf{x}_{t+1} \leftarrow \frac{J_t \mathbf{x}_t}{\|\mathbf{x}_t\|}$
- 8: **end for**
- return** :  $\eta_T$

---

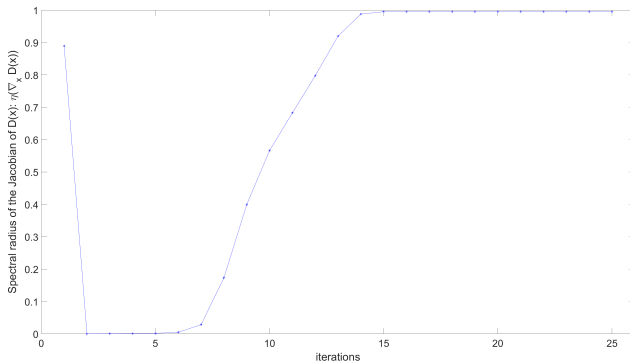


Figure 3: The power iteration method applied on the Jacobian of the denoiser shows that the spectral radius of the latter is lower than one.

## 2. Parameters

In Table 1, we invite the reader to refer to the work of [2], where the parameters used for the baselines are explained in

more details.

In Table 2, to design a super-resolution reconstruction set up, it is important to have a ratio larger than one between the input pixel size of the projection and the reconstructing voxel size.

## 3. Additional results

We provide the results of the **FZP8** reconstructions using all methods (Figure 4). While our proposed method is providing similar results than the PSART-STP, it has 4.5 times lower memory footprint. In the Figure 5, we show 3D rendering visualization of the reconstruction of all datasets using our approach.

A visualization of the **Toothbrush** from the axial plane is given in Figure 6. We can see clearly a better qualitative reconstruction with our method, in comparison to PSART-ATV and PSART-STP approaches.

Finally, a quantitative (PSNR and SSIM) comparison for the real scanned data is provided in Figure 7. Note that these metrics are computed using a reference reconstruction which is not the exact ground truth, but a PSART-ATV reconstruction using higher resolution input projections.

Table 2: CT Parameters for each dataset.

Parameter	FZP2	FZP4	FZP8	Toothbrush	Ropeball	Fan
SID (mm)	1000	1000	1000	243.8	331.457	705.872
SDD (mm)	1536	1536	1536	983	1009.27	1009.27
Detector pixel	$1024 \times 1024$	$1024 \times 1024$	$1024 \times 1024$	$1916 \times 1536$	$1910 \times 1524$	$1910 \times 1524$
Detector pixel size(mm)	0.4	0.4	0.4	0.127	0.127	0.127
Input pixel	$128 \times 128$	$128 \times 128$	$128 \times 128$	$477 \times 381$	$159 \times 127$	$955 \times 762$
Input pixel size (mm)	3.2	3.2	3.2	0.508	1.524	0.254
Image downsampling factor	8	8	8	4	12	2
X-ray penetration (kV)	NA	NA	NA	32	90	90
X-ray intensity ( $\mu A$ )	NA	NA	NA	421	135	100
Reconstruction volume size	$256 \times 256 \times 256$	$512 \times 512 \times 512$	$1024 \times 1024 \times 1024$	$690 \times 669 \times 776$	$290 \times 350 \times 300$	$285 \times 762 \times 233$
Voxel size (mm)	1	0.5	0.25	0.0377	0.1168	0.177
Number of projections	180	180	180	360	720	187

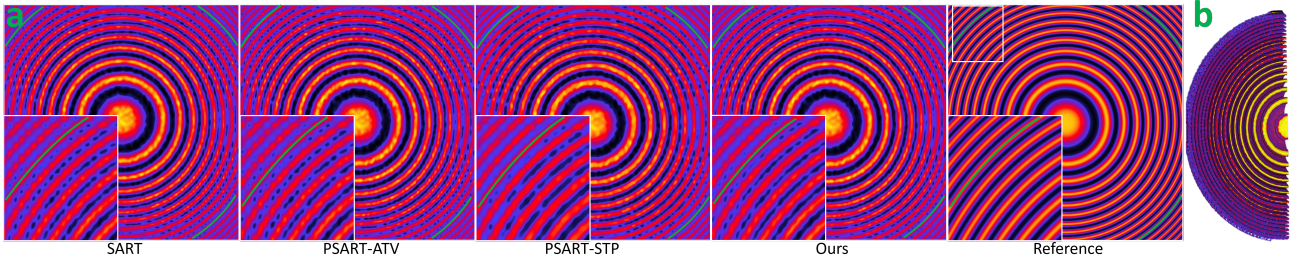


Figure 4: Comparison results for the reconstruction of the Fresnel Zone Plate using 2D cross-sections. (a) FZP8: reconstruction with a  $\times 8$  super-resolution. (b) 3D rendering of the FZP8 using Ours.

## References

- [1] Yaniv Romano, Michael Elad, and Peyman Milanfar. The little engine that could: Regularization by denoising (RED). *SIAM Journal on Imaging Sciences*, 10(4):1804–1844, 2017. [1](#)
- [2] Guangming Zang, Mohamed Aly, Ramzi Idoughi, Peter Wonka, and Wolfgang Heidrich. Super-resolution and sparse view CT reconstruction. In *Proc. ECCV*, pages 137–153, 2018. [2](#)

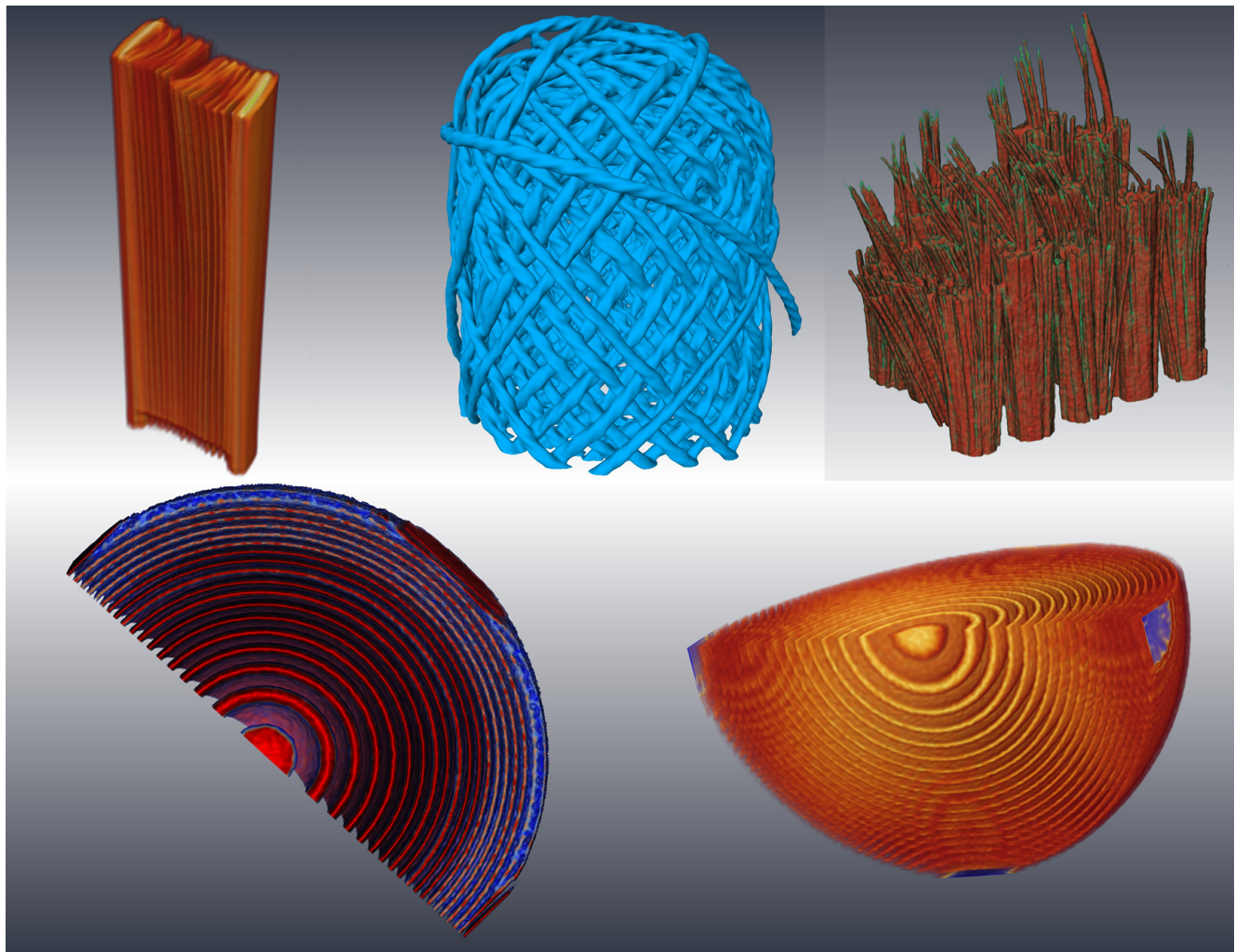


Figure 5: The datasets reconstruction using our method. **Toothbrush**, **Ropeball**, **Fan**, **FZP2**, **FZP4**, respectively.

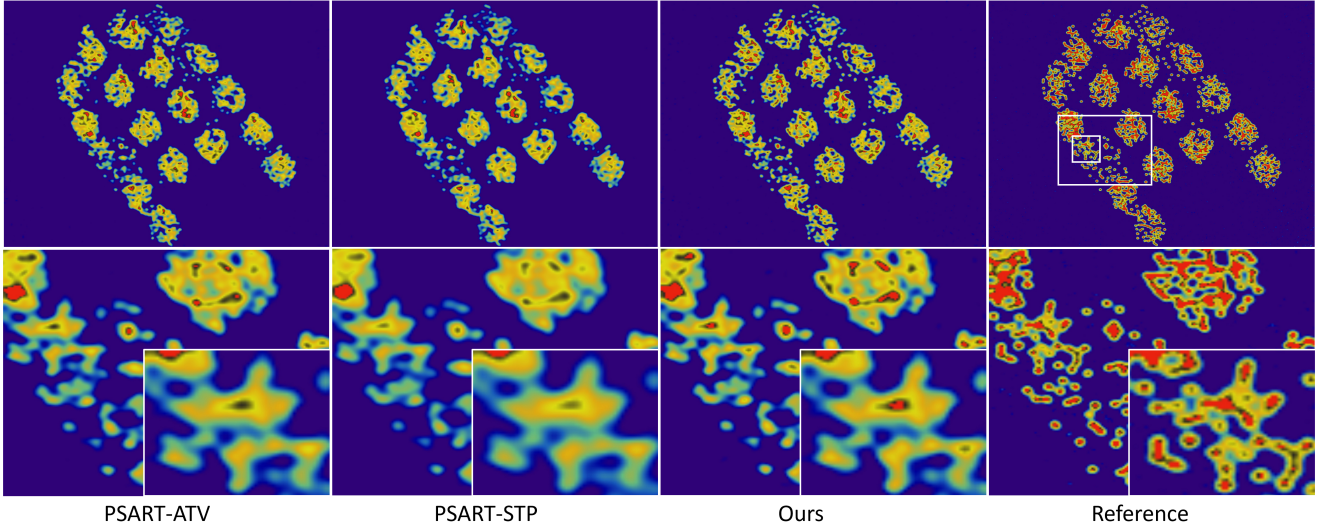


Figure 6: Left to right: representative slice visualization for the toothbrush in the axial plane for the volume and its close up view for the data reconstructed by PSART-ATV, PSART-STP, Ours, and the reference volume, respectively.

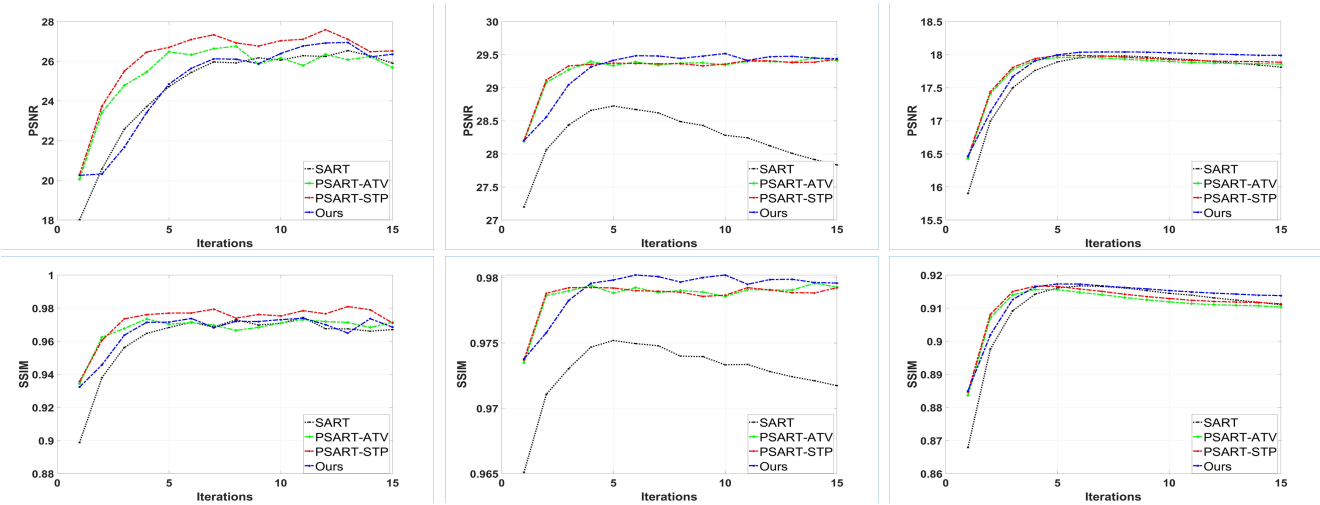


Figure 7: PSNR and SSIM results for the real datasets (from left to right): **Toothbrush**, **Ropeball**, and **Fan**.